Unidimensional forced convection generalized Graetz solutions

Martin Rudkiewicz, Gérald Debenest, Franck Plouraboué, Franck David

SoftwareX 27 (2024) 101834

Contents lists available at ScienceDirect

SoftwareX

journal homepage: www.elsevier.com/locate/softx

Original software publication

Unidimensional forced convection generalized Graetz solutions

Martin Rudkiewicz [a,b], Gérald Debenest [b,*], Franck Plouraboué [b], Franck David [a]

[a] EDF Lab Chatou, 6 Quai Watier, 78400 Chatou, France
[b] IMFT, Institut de Mécanique des Fluides de Toulouse, Université de Toulouse, CNRS, Toulouse, France

ARTICLE INFO

Keywords:
Heat transfer
Numerical method
Generalized Graetz decomposition

ABSTRACT

Heat exchangers are essential in daily life and industries, but evolving demands, like miniaturization and electrification, challenge traditional designs. The Generalized Graetz Decomposition method offers a powerful solution, capable of efficiently modeling heat exchangers, even under these new conditions. Unlike conventional approaches, it generates analytical expressions that require minimal meshing, reducing computational costs. It accounts for all diffusion components, facilitating realistic modeling of low-velocity flows. This method provides a versatile tool for various boundary conditions. The software based on this method simplifies heat exchanger analysis, enables parametric studies, and has the potential to help heat exchanger design, impacting both research and industry.

Code metadata

Current code version	v1.0
Permanent link to code/repository used for this code version	https://github.com/ElsevierSoftwareX/SOFTX-D-24-00103
Permanent link to Reproducible Capsule	none
Legal Code License	GNU general public license (http://www.gnu.org/copyleft/gpl.html)
Code versioning system used	none
Software code languages, tools, and services used	Maple
Compilation requirements, operating environments & dependencies	Maplesoft
If available Link to developer documentation/manual	none
Support email for questions	gerald.debenest@toulouse-inp.fr

1. Motivation and significance

Heat exchangers are ubiquitous in many various industrial applications. They find applications across multiple domains, including transportation, electronic devices, cooling and heating systems [1], chemistry [2], and the agri-food industry [3,4]. These devices are fundamental for efficiently transferring thermal energy within systems of all sizes. In the current era of energy management and optimization, having precise tools for describing and predicting their behavior is of utmost importance. This is why, since numerical simulations are faster and less costly than empirical experimental essays, they are used in many cases in the design strategy [5,6], although not always being able to account for every physical mechanisms involved.

Extensive analytical, numerical, and experimental research has been dedicated to the study of heat exchangers. However, recent trends in miniaturization and electrification have led to an increase in the heat flux that heat exchangers must manage, often surpassing the capabilities of traditional technologies. As a result, new designs have emerged, featuring compact dimensions, smaller footprints [7], and innovative phase change flows [8] or using non Newtonian fluid such as proposed in [9] or [10].

The generalized Graetz decomposition is a semi-analytical method rooted in the classic Graetz problem [11]. It is designed to solve stationary convection–diffusion problems within extruded-like domains, which are challenging to compute accurately due to their highly hyperbolic nature. These problems can typically be solved analytically in the convection dominated limit -neglecting longitudinal diffusion-, or numerically using discretization methods, which can be computationally intensive. For instance, achieving accurate results with finite volume or finite difference methods often hinges on high-quality meshing, which can be demanding for high-velocity flows, domains with high

* Corresponding author.
E-mail addresses: martin.rudkiewicz@toulouse-inp.fr (M. Rudkiewicz), gerald.debenest@toulouse-inp.fr (G. Debenest).

https://doi.org/10.1016/j.softx.2024.101834
Received 17 February 2024; Received in revised form 21 May 2024; Accepted 23 July 2024
Available online 1 August 2024

aspect ratios, or large volumes. The Generalized Graetz Decomposition offers several advantages, chief among them being the generation of an analytical expression that requires, at most, a 2D meshing of the extruded base and remains independent of the domain size in terms of computational cost [12] or [13] Moreover, unlike other analytical solutions that are restricted to high Péclet flows, it accounts for all range of diffusion [14], facilitating a realistic visualization of heat transfers in scenarios with low-velocity flows and conjugated problems. Lastly, this method equips users with a versatile tool for solving various spatially-dependent boundary conditions, including Neumann, Dirichlet, and Robin-Fourier conditions, in contrast to other solutions tailored to specific boundary conditions [15]. The subsequent sections will delve into the resolution of the Navier–Stokes energy equation using the Generalized Graetz Decomposition and its practical implementation in various configurations.

2. Software description

2.1. Generalized Graetz theory

In the Generalized Graetz method, the domain $\mathcal{V}$ is defined as $\mathcal{V} = \Omega \times [a, b]$, where $[a$ and b are real numbers. In other words, the volume is obtained by extending the base Ω along a specific direction, z, over a range $[a, b]$, which could be infinite, i.e. a or $b \to \pm\infty$. Analytical expressions for eigenmodes (3) are feasible only for ducts consisting of concentric layers or plate geometries formed by stacking infinite planes.

Under the following assumptions:

1. The domain is invariant in the z direction.
2. The solution is stationary.
3. Velocity is parallel to the z direction.
4. Thermodynamic properties (including velocity profile) do not depend on the z direction.
5. Lateral boundary conditions are either non-homogeneous Dirichlet or Neumann and depend only on z.

The stationary dimensionless energy convection–diffusion problem is expressed as:

$$\frac{1}{2} w_f(r) \frac{\partial T_f}{\partial z} - \frac{1}{\mathrm{Pe}} \Delta T_f = 0 \tag{1}$$

In (1), the spatial variables, namely the radial and axial coordinates, the length of the domain, and the outer radius, $\tilde{r}$, $\tilde{z}$, $\tilde{L}$, and $\tilde{R}_0$, are rescaled by the inner radius $\tilde{R}$ (or the half height of the channel). The non-dimensional velocity w_f is defined with respect to the mean velocity $\tilde{W}_s$, as $w_f(r) = \tilde{W}(r)/\tilde{W}_s$. For Poiseuille flow, w_f takes the form $w_f = a(1 - r^2)$, with $a = 2$ for circular ducts and $3/2$ for plate channels. The Péclet number $Pe = \tilde{W}_s 2\tilde{R}/\alpha_f$ compares convection effects to thermal conduction, with thermal diffusivity defined as $\alpha_f = k_f/(\rho c_p)$. The dimensionless fluid temperature T_f is expressed as $T_f = (\tilde{T} - \tilde{T}_0)/\Delta\tilde{T}_h$, where $\Delta\tilde{T}_h$ and $\tilde{T}_0$ represent characteristic temperature differences and temperatures in the problem, respectively. The non-dimensional thermal conductivity is defined as $\kappa = \tilde{k}/k_f$. Within each compartment of the domain, properties may change, particularly the velocity, which is set to 0 inside solid compartments.

The solution to Eq. (1) relies on the properties of the associated operator, which guarantees the existence of an orthogonal basis of eigenvectors. With T_i as the ith eigenmode and λ_i as the associated eigenvalue, the temperature field is given by:

$$T(r,z) = \sum_{i\in\mathbb{Z}^*} \alpha_i c_i(z) T_i(r) e^{\lambda_i z} + f(z) + \sum_{i\geq 0} x_i T_i(r) e^{\lambda_i (z - z_{in})} + \sum_{i<0} x_i T_i(r) e^{\lambda_i (z - z_{out})} \tag{2}$$

Eigenmodes are divided into two groups based on the sign of their eigenvalues: positive eigenvalues correspond to upstream modes with negative indexes, while negative eigenvalues correspond to downstream modes with positive values of i. Due to symmetric lateral boundary conditions, eigenmodes depend solely on the radial coordinate [14]. Furthermore, as shown in [12], these eigenmodes can be expressed as analytical functions of eigenvalues λ_i involving closure functions t_p, as:

$$\forall i \in \mathbb{Z}^* : T_i(r) = \sum_{p=0}^{\infty} t_p(r) \lambda_i^p \tag{3}$$

The closure functions can be evaluated recursively following the relation (4), while conditions between each compartment are imposed by the continuity of thermal heat flux and temperature. In the jth compartment,

$$\Delta t_p = \frac{\mathrm{Pe}_j}{2} w_f(r) t_{p-1} - t_{p-2}, \tag{4}$$

with in each compartment, $\mathrm{Pe}_j = \tilde{W}_{Sj} 2\tilde{R}/\alpha_j$. The closure functions are determined by fluid flow characteristics, material properties, compartment organization, and lateral boundary conditions, ensuring the temperature field's shape and satisfaction of Eq. (1). In Eq. (4), an infinite sum is mathematically prescribed, but numerically only a finite number N of closure functions is computed, defining the method's order. At this stage, the amplitudes x_i remain unknown, since the inlet and outlet boundary conditions are not yet specified.

2.2. Resolution

To determine the coefficients x_i, appropriate values satisfying the inlet and outlet conditions, a unique cost function is minimized, as considered in [12]. This cost function is specific to a given class of inlet/outlet conditions. Several examples illustrating its formulation are presented in Section 3.

Fig. 1 illustrates the structure of the temperature decomposition in a counter-current heat exchanger with five compartments (two fluid compartments and three solid walls). The temperature field is divided into two components: Part A, which accounts for the impact of lateral boundary conditions, and Part B, which enforces conditions at the inlet and outlet of the domain. Part B is further subdivided into two sums: negative indices control the behavior at the outlet of the domain, and positive indices govern the inlet conditions. Similar to a Fourier decomposition, the amplitudes correspond to the projection of the conditions onto the basis of eigenvectors.

2.3. Software architecture

The software is organized into five sections:

1. *Configuration and Setup*: in this initial section, users can specify various parameters, including the number of compartments, their dimensions and arrangement, the various velocity profiles, and material properties (thermal conductivity, thermal capacity, and density). Additionally, boundary conditions and numerical parameters, such as the method's order and digital precision, are prescribed.
2. *Spectrum and Eigenmodes Computation*: this section is dedicated to computing the spectrum and eigenmodes. It begins by solving the differential Eq. (4) from solving the closure functions in each compartments. The eigenvalues are then deduced from these closure functions, considering the type of lateral boundary conditions. Finally, the eigenmodes are assembled as in (3).
3. α_i *and* $c_i(z)$ *evaluation*: calculate α_i and $c_i(z)$, based on the Dirichlet or Neumann nature of the lateral conditions. These quantities involve convolution products which can be computed analytically if the longitudinal applied boundary conditions are given analytically.
4. *Cost Function Minimization*: regarding this step, the software constructs and minimizes the cost function, resulting in the

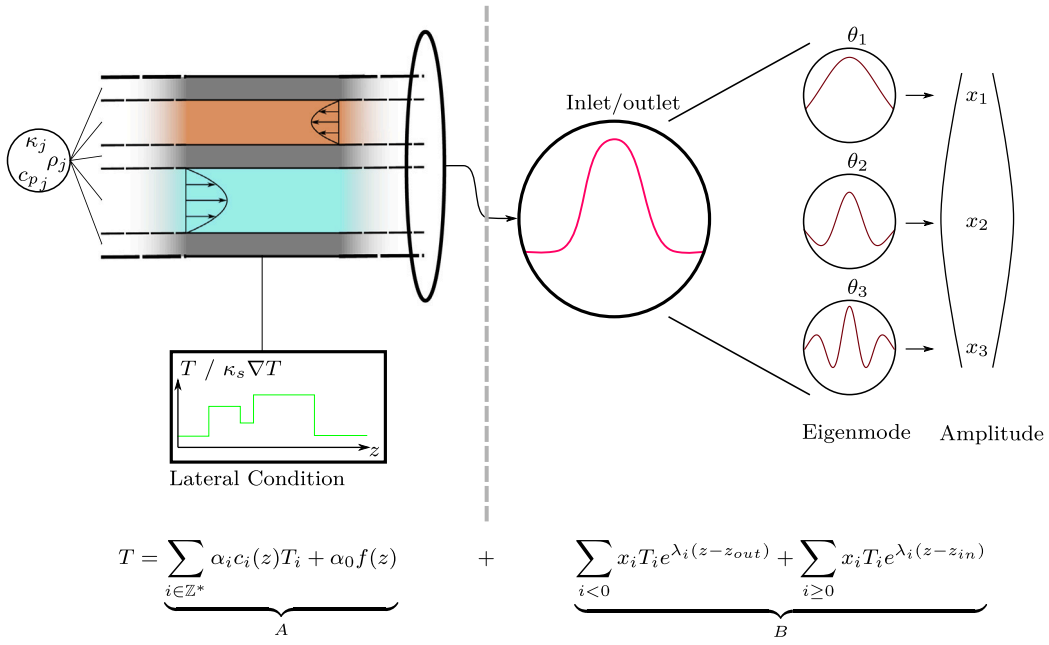

Fig. 1. Structure of the temperature field.

determination of the missing amplitudes x_i. The minimization of this cost function leads to the resolution of a linear system defined over the amplitude vector **x**, i.e, **Mx** = **B**. Notably, the matrix **M** depend on cross-projections between the eigenmodes and can be evaluated whatever the applied inlet or outlet conditions (thus it can be pre-computed and stored if one would like to explore a lot of inlet/outlet conditions). On the contrary vector **B** depends on the projections between the eigenmodes and applied inlet/outlet conditions.

5. *Temperature Field Assembly*: this final section assembles the temperature field, making it ready for post-processing, exportation, and grid evaluation, since the code provides a mesh-less analytical solution.

3. Illustrative examples

To illustrate the range of possibilities within the field, we provide detailed results in three examples. The first two examples present local temperature profiles within channels, with the first one involving a channel without solid walls and the second featuring a channel with solid walls. The third example delves into global measurements, specifically the characterization of the efficiency of a co-current heat exchanger. A validation procedure has been rigorously followed in [16] and readers can refer to this recent study where some natural heat transfer loops have been studied compared to CFD tools.

3.1. Imposing a Gaussian inlet temperature profile

This example demonstrates how to apply an inlet boundary condition, such as a Gaussian temperature profile, to a straightforward circular semi-infinite channel with fixed wall temperature. In this case, the channel extends from $z \in [0, +\infty[$. A laminar velocity profile is imposed within this single-compartment domain, and the wall temperature $\tilde{T}_w$ remains constant, serving as a reference temperature.

Consequently, the non-dimensional temperature field adheres to the following conditions: $T(r, 0) = \exp(-10r^2)$ and $T(1, z) = 0$. The outlet of the channel at $z \to +\infty$ does not necessitate a specific boundary condition, and its temperature T_∞ is an outcome of the problem.

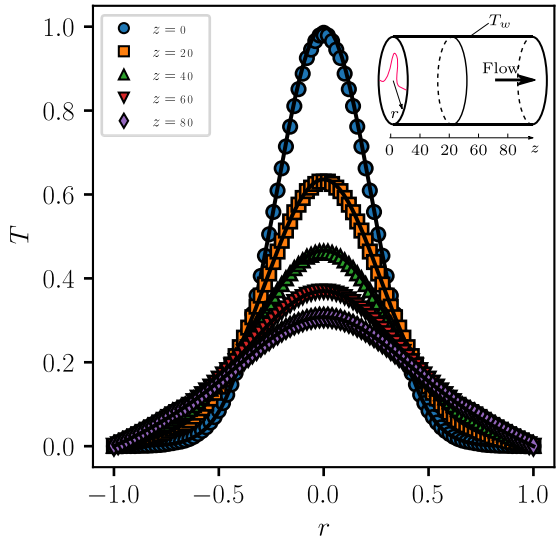

Fig. 2. Temperature profiles in a circular tube with prescribed wall and inlet temperatures. Black lines represent the results obtained using the Graetz model, while the symbols illustrate those obtained through a CFD simulation performed with Code_Saturne.

For a Dirichlet lateral boundary condition [15], we have the following equations:

$$\begin{aligned} &\forall i \in \mathbb{Z}^* : \alpha_i = -\frac{2\pi R}{\lambda_i^2} \frac{dT_i}{dr}(R) \; ; \; \alpha_0 = 1 \; ; \; f(z) = T_w = 0 \\ &\forall i > 0 : c_i(z) = -\int_0^z \frac{dT_w}{dz} e^{\lambda_i (z-\xi)} d\xi \\ &\forall i < 0 : c_i(z) = \int_z^{+\infty} \frac{dT_w}{dz} e^{\lambda_i (z-\xi)} d\xi \end{aligned} \tag{5}$$

In this particular case, part A of the temperature field (discussed in Fig. 1) is reduced to zero. The determination of the amplitudes x_i in part B is based on the minimization of the cost function $F(\mathbf{x}) = \int_0^1 r(T(r, 0) - T_{in})^2 dr$. Fig. 2 presents successive radial temperature profiles within the

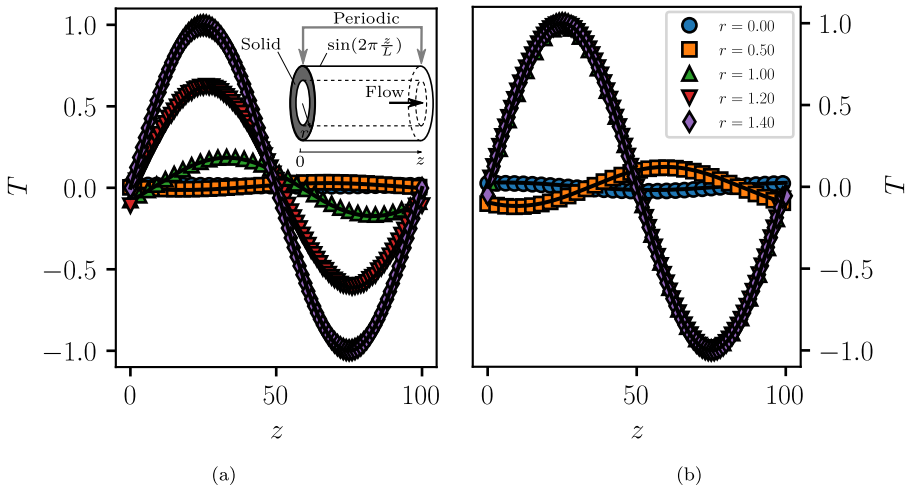

Fig. 3. Temperature profiles in a circular channel with a solid wall, $1 \leq r \leq 1.4$, the temperature is imposed at the outer extremity of the wall, $r = 1.4$, with a periodic condition in z. Black lines highlight the profiles obtained through the Graetz method ; the symbols, those with Code_Saturne. Two configurations are considered with the same conditions except for the thermal conductivity ratio between the fluid and the solid wall, κ_s, respectively imposed at two values, $\kappa_s = 0.25$, in 3(a) and $\kappa_s = 678$, in 3(b). (For interpretation of the references to color in this figure legend, the reader is referred to the web version of this article.)

channel at increasing axial positions. The results obtained with the generalized Graetz model are overlaid with those from a CFD simulation of the same configuration, demonstrating excellent agreement between the two methods. Both indicate the widening of the Gaussian profile along the channel due to thermal radial diffusion.

3.2. Effect of solid wall thermal conductivity

In this example, we demonstrate the use of a z-dependent lateral boundary condition within a two-compartment domain. The domain consists of a finite circular channel with a solid wall. At the outer border of the wall ($r = R_0$), a sinusoidal temperature profile, $\tilde{T}_w = \Delta\tilde{T}_h \sin\left(\frac{2\pi\tilde{z}}{\tilde{L}}\right) + \tilde{T}_0$, is imposed, while a periodic condition is applied between the outlet and the inlet of the tube at $z = 0$ and $z = L$. The inner compartment ($0 \leq r \leq 1$) features fluid flow according to the Poiseuille law (but any analytical radial dependence for the longitudinal velocity field c an be chosen), while the outer compartment ($1 \leq r \leq R_0$) represents the solid wall. Using the non-dimensional expression of the lateral condition, $T_w = \sin\left(\frac{2\pi z}{L}\right)$ and the relations detailed in (5), the $c_i(z)$ are no longer equal to zero.

For the B part of the temperature field, the amplitudes can be determined analytically [17]:

$$\begin{aligned} \forall i \geq 0 : x_i &= \alpha_i \frac{c_i(L) - c_i(0)}{1 - e^{\lambda_i L}} \\ \forall i < 0 : x_i &= \alpha_i \frac{c_i(L) - c_i(0)}{e^{-\lambda_i L} - 1} \end{aligned} \tag{6}$$

In Fig. 3, we present five temperature profiles along the channel for two values of the wall thermal conductivity. Generally, the temperature variation in the fluid (blue and orange symbols) remains slightly lower than in the solid (red and purple symbols). On the left, a significant radial temperature gradient within the wall is observed, which is due to a relatively insulating material. On the other side, when the wall is an excellent thermal conductor, it is nearly impossible to distinguish the temperature profile in the solid, indicating that the temperature is almost constant in the radial direction. As in Section 3.1, a comparison between the results obtained with the Graetz methodology and those from a CFD simulation shows a very good agreement.

3.3. Characterizing the efficiency of a parallel co-current heat exchanger

This example shows the implementation of a finite co-current heat exchanger with semi-infinite inlet and outlet channels. In practice,

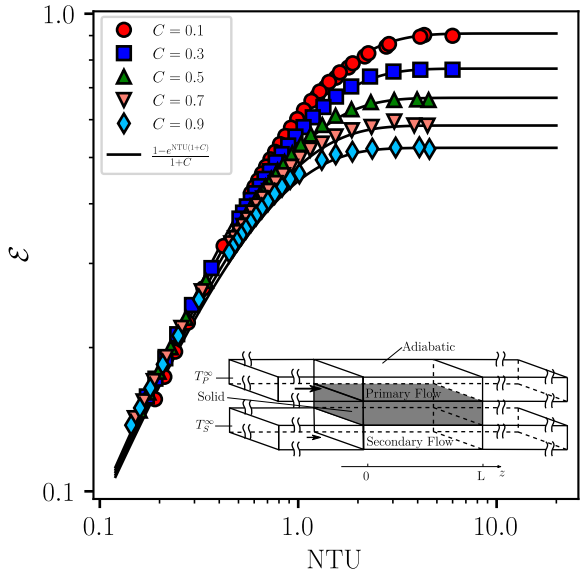

Fig. 4. Variation in the efficiency of a co-current plate heat exchanger versus the Number of Transfer Units (NTU) for different mass flow ratios between 0.1 and 0.9. Black lines represent the analytical solution for a 2D co-current heat exchanger, while the symbols depict the results achieved with the generalized Graetz decomposition.

specifying inlet and outlet conditions can be a challenging aspect of simulating heat exchangers. While it is straightforward to impose a temperature profile, it often does not account for the effect of thermal diffusion, which can alter the imposed temperature. To address this concern, inlet conditions need to be placed at a significant upstream position, which, in turn, increases the domain's volume and computational cost in the case of CFD simulations. Outlet conditions can be equally challenging, as the shape of the outlet temperature profile is typically a result of the simulation and cannot be prescribed in advance. The common solution is to extend the outlet of the heat exchanger far enough from the heat exchanger to allow the temperature profile to establish. In contrast, solving this configuration with the generalized Graetz decomposition incurs only a modest additional cost, as the domain's length does not significantly influence the numerical cost of the Graetz method [18].

In this configuration, the heat exchanger comprises two fluid channels, $-2H_{II} - h \leq y \leq -h$ and $h \leq y \leq 2H_I + h$, separated by a solid wall ($-h \leq y \leq h$). The channel with the higher mass flow is identified as the primary channel, and the other as the secondary channel. The semi-infinite tubes that enter and exit the heat exchanger, along with the heat exchanger's extremities, are insulated. Inlet temperatures are imposed at $-\infty$ for both the primary, T_I^∞, and the secondary, T_{II}^∞, channels.

For Neumann lateral boundary conditions, the coefficients α_i and c_i are determined as follows [15]:

$$\begin{aligned}
&\forall i \in \mathbb{Z}^* : \alpha_i = \frac{2\pi R}{\lambda_i} T_i(R) \; ; \; \alpha_0 = \frac{\mathcal{P}}{\int_{-2H_{II}-h}^{2H_I+h} \frac{\mathrm{Pe} w_f}{2\kappa} dy} \; ; \; f(z) = \int \varphi_w dz = 0 \\
&\forall i > 0 : c_i(z) = -\int_0^z \varphi_w e^{\lambda_i(z-\xi)} d\xi \\
&\forall i < 0 : c_i(z) = \int_z^{+\infty} \varphi_w e^{\lambda_i(z-\xi)} d\xi \\
&\text{with } \mathcal{P} = \int_{\partial\Omega} dl, \text{ and } \varphi_w = \kappa \frac{\partial T}{\partial y}_{|\partial\Omega}
\end{aligned} \tag{7}$$

Since the lateral boundaries are adiabatic, the A contribution to the temperature field equals zero. However, the amplitudes' determination is more complex in this case. In addition to the inlet conditions at $-\infty$, there are four junctions between the semi-infinite channels and the inlets and outlets of the heat exchanger. Each junction enforces the continuity of temperature and heat flux, resulting in a cost function:

$$\begin{aligned}
F(\mathbf{x}) = &\int_{\Gamma_0^I \cup \Gamma_0^{II}} (T_u - T_{exc})^2 + \left(\frac{\partial T_u}{\partial z} - \frac{\partial T_{exc}}{\partial z} \right)^2 d\Omega \\
&+ \int_{\Gamma_0^s} \left(\kappa_s \frac{\partial T_{exc}}{\partial z} \right)^2 d\Omega \\
&+ \int_{\Gamma_L^I \cup \Gamma_L^{II}} (T_{exc} - T_d)^2 + \left(\frac{\partial T_{exc}}{\partial z} - \frac{\partial T_d}{\partial z} \right)^2 d\Omega \\
&+ \int_{\Gamma_L^s} \left(\kappa_s \frac{\partial T_{exc}}{\partial z} \right)^2 d\Omega
\end{aligned} \tag{8}$$

Here, $\Gamma_{0/L}^{I/II/s}$ represents the normal section to z of one of the compartments at either $z = 0$ or $z = L$. The subscripts u, d, and exc correspond to upstream, downstream, and heat exchanger, respectively, and denote the volumes placed before $z \in]-\infty, 0]$, after $z \in [L, +\infty[$, and within the heat exchanger $z \in [0, L]$. Fig. 4 illustrates the efficiency of the heat exchanger, $\mathcal{E} = (\langle T_{II} \rangle(L) - T_{II}^\infty)/(T_I^\infty - T_{II}^\infty)$, where $\langle T_{II} \rangle = \int_{\Gamma^{II}} w_f T d\Omega / \int_{\Gamma^{II}} w_f d\Omega$, as a function of the Number of Transfer Units (NTU), defined by (9), for various mass flow ratios, $C = (\tilde{W}_{SII} \tilde{H}_{II})/(\tilde{W}_{SI} \tilde{H}_I)$. The results obtained with the generalized Graetz decomposition are in excellent agreement with the analytical solution [3].

$$NTU = \int_0^L \frac{\kappa_s \frac{\partial T}{\partial y}}{\langle T_I \rangle - \langle T_{II} \rangle} dz \frac{k_f}{\tilde{\rho}_{II} \tilde{W}_{SII} \Gamma^{II} \tilde{c}_{pII}} \tag{9}$$

4. Impact and conclusion

The implementation of a semi-analytical solution to solve general 2D conjugated heat transfer convection/diffusion has been presented and illustrated. This methodology has undergone successful validation against computational fluid dynamics (CFD) simulations and analytical solutions across a range of configurations.

The analytical expression for temperature, derived from this software, facilitates straightforward and versatile post-processing. This becomes particularly valuable when evaluating temperature gradients or collecting global measurements based on integrated variables. Notably, the Generalized Graetz modes method proves highly adaptable for deducing simplified expressions or asymptotic behaviors in specific scenarios [19].

One distinctive advantage of the Generalized Graetz Decomposition is the elimination of a meshing stage, which significantly reduces the computational cost, making it especially attractive for large domains. This feature proves invaluable when dealing with the imposition of inlet and outlet conditions. However, it is essential to acknowledge that the quality of these boundary conditions directly hinges on the method's order and the complexity of the conditions. For instance, imposing a variety of conditions in a multi-compartment domain may necessitate a higher-order method compared to a single-compartment setup.

Another key attribute of the Graetz Method is its capacity to account for thermal conduction along the flow direction. This capability is crucial for modeling entrance regions, thick solid walls, and low Péclet number flows — characteristics commonly encountered in miniaturized or micro-scale heat transfer problems.

Furthermore, the Generalized Graetz Modes offer a notable advantage in terms of computational efficiency, making it an attractive option for parametric optimization processes, code validations and the generation of extensive datasets solutions. The combination of low computational time and analytical rigor positions this method as a powerful tool in the field of thermal analysis.

CRediT authorship contribution statement

Martin Rudkiewicz: Writing – original draft, Validation, Software, Investigation, Conceptualization. **Gérald Debenest:** Writing – review & editing, Supervision. **Franck Plouraboué:** Writing – review & editing, Supervision, Software, Investigation, Conceptualization. **Franck David:** Writing – review & editing, Supervision.

Declaration of competing interest

The authors declare the following financial interests/personal relationships which may be considered as potential competing interests: Martin Rudkiewicz reports financial support was provided by EDF Research and Development Chatou Site. If there are other authors, they declare that they have no known competing financial interests or personal relationships that could have appeared to influence the work reported in this paper.

Data availability

Data will be made available on request.

Acknowledgments

We thanks Dr. C. Pierre from UPPA Univ., Pau, France, for sharing his maple code that we have adapted for various configurations.

References

[1] Ragueb H, Mansouri K. Exact solution of the Graetz–Brinkman problem extended to non-Newtonian nanofluids flow in elliptical microchannels. J Engrg Math 2023;140(1):10.
[2] Gururajan V, Som S. Numerical solutions to the reactive Graetz problem for CO2 capture. Carbon Capt Sci Technol 2022;5:100071.
[3] Shah R, Sekulic D. Fundamentals of heat exchanger design. Wiley; 2003.
[4] Li Q, Flamant G, Yuan X, Neveu P, Luo L. Compact heat exchangers: A review and future applications for a new generation of high temperature solar receivers. Renew Sustain Energy Rev 2011;15(9):4855–75.
[5] Aslam Bhutta MM, Hayat N, Bashir MH, Khan AR, Ahmad KN, Khan S. CFD applications in various heat exchangers design: A review. Appl Therm Eng 2012;32:1–12.
[6] Abeykoon C. Compact heat exchangers – Design and optimization with CFD. Int J Heat Mass Transfer 2020;146:118766.
[7] Hesselgreaves JE, Law R, Reay D. Compact heat exchangers: Selection, design and operation. 2nd ed. Butterworth-Heinemann; 2017, p. 1–33.

[8] Bergles AE. High-flux processes through enhanced heat transfer. 2003.
[9] Khan MWS, Ali N, Asghar Z. Thermal and rheological effects in a classical Graetz problem using a nonlinear Robertson-Stiff fluid model. Heat Transfer 2021;50(3):2321–38.
[10] Khan MWS, Asghar Z, Shatanawi W, Gondal MA. Thermal entry problem for a tube with prescribed heat flux condition using viscoplastic fluid: An extended Graetz problem for Casson fluid with axial conduction and viscous dissipation. ZAMM-J Appl Math Mech (Z Angew Math Mech) 2024;e202300109.
[11] Graetz vL. Über die wärmeleitungsfähigkeit von flüssigkeiten. Ann Phys, Lpz 1885;261(7):337–57.
[12] Pierre C, Bouyssier J, De Gournay F, Plouraboué F. Numerical computation of 3D heat transfer in complex parallel heat exchangers using generalized Graetz modes. J Comput Phys 2014;268:84–105.
[13] Seco-Nicolás M, Alarcón M, Luna-Abad JP. 3D numerical simulation of laminar forced-convection flow subjected to asymmetric thermal conditions. An application to solar thermal collectors. Sol Energy 2021;220:230–45.
[14] Pierre C, Plouraboué F. Analytical properties of Graetz modes in parallel and concentric configurations. Meccanica 2020;55(8):1545–59.
[15] Bouyssier J, Pierre C, Plouraboué F. Mathematical analysis of parallel convective exchangers with general lateral boundary conditions using generalized Graetz modes. Math Models Methods Appl Sci 2014;24(04):627–65.
[16] Plouraboué F, Rudkiewicz M, David F, Neau H, Debenest G. Natural convective loops heat transfer scaling analysis. Int J Heat Mass Transfer 2024;218:124743.
[17] Fehrenbach J, De Gournay F, Pierre C, Plouraboué F. The generalized Graetz problem in finite domains. SIAM J Appl Math 2012;72(1):99–123.
[18] Dichamp J, De Gournay F, Plouraboué F. Theoretical and numerical analysis of counter-flow parallel convective exchangers considering axial diffusion. Int J Heat Mass Transfer 2017;107:154–67.
[19] Plouraboué F, Pierre C. Stationary convection–diffusion between two co-axial cylinders. Int J Heat Mass Transfer 2007;50(23–24):4901–7.